Identifying Interaction Phenomena among Converters

Yahya LAMRANI, Frédéric COLAS, Carmen CARDOZO, Thibault PREVOST and Xavier GUILLAUD
Univ. Lille ULR 2697 - L2EP, Arts et Métiers Institute of Technology, Centrale Lille, Junia, F-5900 Lille, France
RTE R&D, 92919 La Défense, France

ABSTRACT – Stability analysis of power electronics converters is necessary to ensure a reliable future power system. Most existing studies use a Thévenin equivalent setup. This paper presents the limits of this test setup and suggests an alternative allowing to better highlight the instability and interaction phenomena.

Key words—Small-signal stability, State-Space models, Interaction phenomena, Grid-following control.

1. INTRODUCTION

The integration of power electronics converters in power systems has brought new challenges to the stability of the electrical grid. It has been recognized by several stakeholders that the conventional control of converters leads to a decrease of the system stability [1], the conventional control referring to Grid-Following (GFL) control. In fact, it has been reported that Grid-Following converters encounter small-signal stability issues in weak grid [2] and may lose synchronism by interacting with other converters in electrical proximity of their Point of Common Coupling (PCC) [3]. These interactions can have a significant impact on the stability, reliability, and efficiency of the power system, making it important to study and understand them in order to ensure safe and efficient operation of the power system. Most small-signal stability studies found in literature are conducted using a Thévenin equivalent test setup [2], [4] to study GFL-controlled converters in various grid strength conditions. The present work shows the limit of this setup with regards to its capacity to confirm the claims concerning small-signal stability and interaction of the GFL control and proposes an alternative test setup to serve multiple purposes:

- Highlight the small-signal stability limit of GFL control
- Analyze the interaction phenomena among converters
- Test the interaction indicators found in the literature

This paper is organized as follows: Section 2 presents the GFL control structure tuning and its behavior in a Thévenin equivalent setup. Section 3 presents the proposed setup and uses it to investigate the underlying instability mechanisms. Section 4 confronts the interaction phenomena analysis conducted in this paper to the interaction indicators found in literature. Finally, Section 5 concludes the paper.

2. GRID-FOLLOWING CONVERTER IN A THÉVENIN EQUIVALENT

This section studies the small-signal stability of a GFL-controlled Voltage Source Converter (VSC) connected to the grid, modelled by a Thévenin equivalent as shown in figure 1. The grid impedance is chosen to reflect the grid strength, evaluated by the Short-Circuit Ratio (SCR). The definition of the SCR is recalled below:

$$SCR = \frac{S_{SC}}{P_n} = \frac{1}{L_g \omega_g} \quad (1)$$

where S_{SC} is the short-circuit power of the grid at the VSC PCC, P_{nom} is the rated power of the VSC, and ω_g, L_g are respectively the grid's frequency and inductance in p.u assuming an inductive impedance for transmission grids.

The circuit parameters and base values, shown in Table 1, describe a transmission grid application.

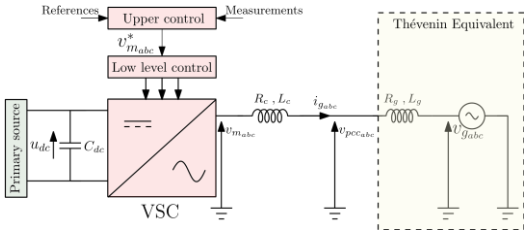

Fig. 1. VSC converter connected to a Thévenin equivalent.

Table 1. Thévenin equivalent setup parameters

Control	Parameter	Value
VSC	S_{nom}, S_b	1.044 GVA
	U_{nom}, U_b	400 kV
	P_{nom}	1 GW
	Q_{max}	300 MVAr
Filter	L_f	0.15 pu
	R_f	0.005 pu
Grid	L_g	1/SCR
	R_g	$L_g/10$

2.1. Grid-Following Control

The control considered in this article is a generic GFL control structure which is synchronized to the grid thanks to a Phase-Locked Loop (PLL). Furthermore, the inputs of the control are filtered to account for the limited bandwidth of the measurement devices, and the modulated voltage references are delayed to account for the effect of the Pulse-Width Modulation. Following the literature recommendation for GFL control tuning in weak grids [4], the parameters of the GFL control are shown in Table 2.

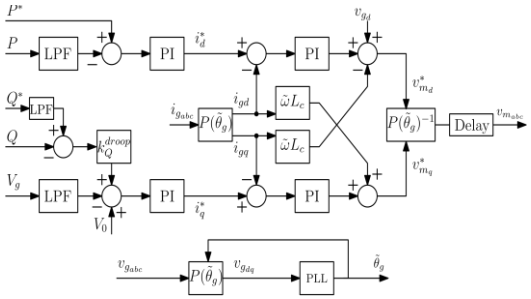

Fig. 2. GFL control structure.

Table 2. GFL control parameters

Control	Parameter	Value
Input filters	ω_{LPF}^{inputs}	10000 rad/s
Outer loops	ω_p	10 rad/s
	ω_v	50 rad/s
	k_Q^{droop}	0.15
	$\omega_{LPF}^{outer\ loops}$	300 rad/s
PLL	ω_n	50 rad/s
	ξ	1
Current loops	ω_{cc}	1200 rad/s
	f_{sw}	2 kHz

2.2. *Static limit of the Thévenin equivalent*

Considering the parameters in Table 1 describing the test setup, it is clear that it is only possible to test the small-signal stability of the GFL-controlled VSC for $SCR \geq 1.35$. Any lower SCR value would lead to a situation where the converter could not transfer its nominal power at the nominal voltage while respecting the reactive power constraints.

However, testing the previously described GFL control at this static limit shows, in figure 3, that the system remains small signal stable. In fact, by considering a small disturbance event such as a $\frac{\pi}{40}$ phase jump of the Thevenin voltage source, the system experiences a momentary overvoltage but successfully regains a steady state operating point. Therefore, the reported instability issues and interaction phenomena cannot be studied using a Thévenin equivalent setup.

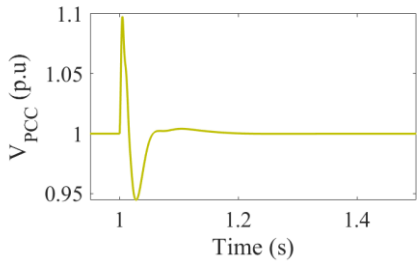

Fig. 3. Time domain reaction of V_{pcc} to a phase jump of v_g

3. Proposed Test Setup

To overcome the limits of the Thévenin equivalent setup, the test setup presented in figure 4 is proposed. The previously studied VSC is split into VSC1 and VSC2, each of a nominal power of $P_{nom}/2$.

Each converter is connected to the grid via overhead lines of varying lengths to reflect a more realistic case where the VSC stations are not equally distanced from the transmission grid. The power can partially circulate from one VSC to another and partially flow to the grid, which lifts the previously identified static constraints.

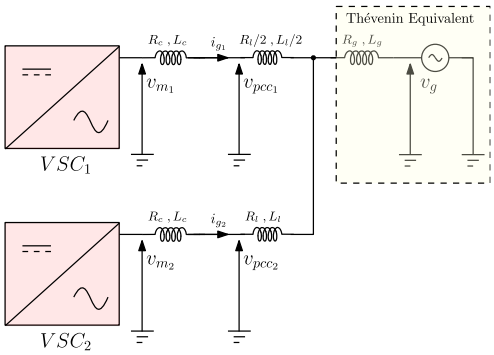

Fig. 4. Proposed alternative setup.

3.1. *Validation of the linearized state-space model*

A state-space model of the setup is constructed and is linearized around various operating points. A first operating point is chosen to validate the linearized state-space model against the non-linear model in time-domain simulation. The details of this first operating point are given in Table 3. As shown in figure 5, the linearized-model accurately replicates the dynamics of the non-linear model for small-signal disturbances and will be used henceforth for the system stability analysis.

Table 3. First operating point parameters

Circuit	Parameter	Value
VSC	$P_{ref}^{VSC_1}$	0.1 pu
	$P_{ref}^{VSC_2}$	0.1 pu
Overhead lines	L_l	0.144 pu
	R_l	0.0072 pu
Grid	L_g	1 pu
	R_g	0.1 pu

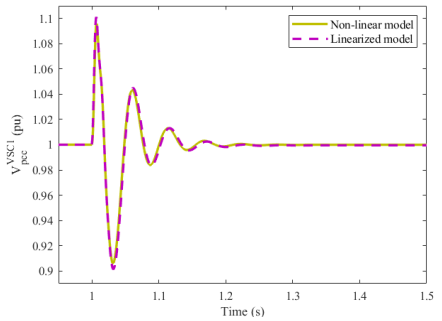

Fig. 5. Time domain comparison of $V_{pcc}^{VSC_1}$ after a $\frac{\pi}{40}$ phase jump of v_g

3.2. *Impact of load flow pattern*

Before varying the operating point of the system with regards to the grid strength, a second operating point is studied to assess the impact of the load flow pattern on the system dynamics so as to ensure that the following findings are not limited to a single load flow pattern.

The second operating point is chosen so as to keep the same power flowing towards the grid. However, VSC1 is now injecting its nominal power (500MW) while VSC2 is absorbing the difference (-300 MW). This could be representative of a case

where VSC1 is a wind farm and VSC2 is a HVDC link partially evacuating the generated power of the wind farm.

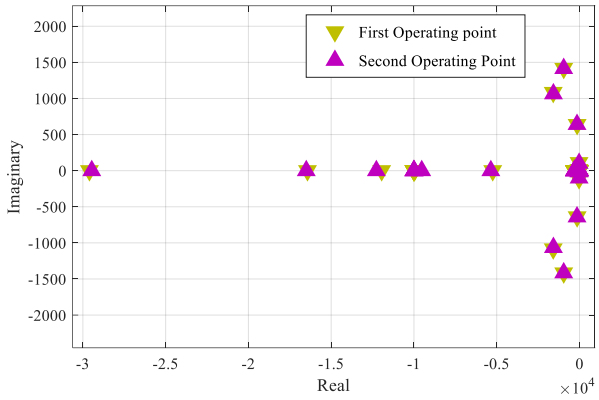

Fig. 6. Comparison of pole maps under two different operating points.

As shown in figure 6, the eigenvalues of both operating points are almost identical.

Furthermore, it can be shown, via time domain simulation, that the stability limit of both operating points with regards to the grid strength is the same. The system oscillations have the same frequency which further supports that the operating points share the same dominant mode.

3.3. Sensitivity to the grid strength

The sensitivity to the grid strength is assessed by analyzing the evolution of the system eigenvalues for increasing values of the grid impedance (decreasing values of the SCR). The first operating point is selected for this analysis. The grid impedance is varied so as to reflect an SCR ranging from 0.5 to 1. Note that it is thanks to the new setup and the chosen power flow that the SCR can reach such values while respecting the static constraints of the circuit.

As figure 7 shows, the system becomes unstable for SCR values lower than 0.65. It is possible to identify the eigenvalues most sensitive to the grid strength on the plot. In fact, two pairs of eigenvalues are identified, with one pair (circled in red) representing the system dominant mode. This dominant mode is extremely sensitive to the grid strength as its real part becomes positive leading to instability. Furthermore, its damping ratio is increased 100 times from SCR = 0.7 to SCR = 1 which significantly impacts the system dynamic performance. Therefore, it is expected that this mode will reflect the mechanisms behind the system sensitivity to the grid strength.

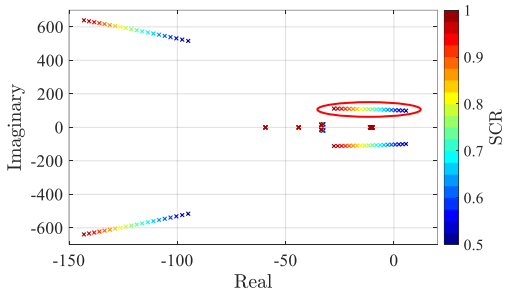

Fig. 7. Parametric sensitivity to the grid strength.

3.4. Analysis of participation factors

The previous study is utilized to understand the interaction phenomena via the analysis of the participation factors of the dominant mode.

In fact, to better understand the underlying instability mechanisms, the contributions of all state variables in the identified dominant mode ($\lambda = -27.11 \pm 111.71i$) are showcased in figure 8.

The participation factors reflect an almost identical contribution of both converters to the dominant mode. The differences stem from the structural choice placing VSC2 electrically further than VSC1 (via the overhead lines) from the stiff voltage source, thus being more susceptible to instability issues. However, the contributions from each converter are the same. First, the PLL-related state variables contribute the most to the dominant mode: this is expected as the PLL is crucial to synchronize the controls but is sensitive to voltage disturbances. The voltage disturbances are in this setup doubled as they originate from the voltage drop over the grid impedance and from the current injection of the other converter. The second most contributing state variable is related to the voltage regulation which is expected as both converters attempt to control the voltage at their respective PCCs which are electrically close. Finally, the filtered inputs and the output delays contribute to the dominant mode, which is logical considering that input filters introduce a delay of the control with regards to the measured signals and delays in controls are known to contribute negatively to stability.

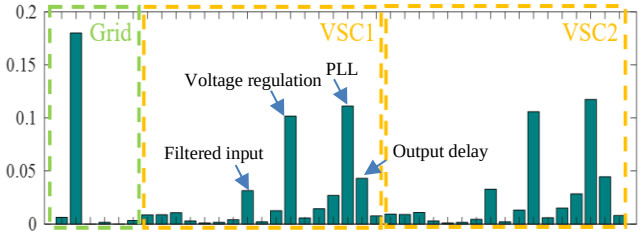

Fig. 8. Participation factors of state variables in identified eigenvalue.

The takeaways from the analysis above are coherent with the literature findings as it has been already reported that the synchronization mechanism and voltage control are closely correlated and lead to interactions between electrically close converters [3], [5]. Thanks to this analysis, the instability origins are highlighted and can be tackled via better tuning (i.e., slower PLL) or by considering different controls providing a mitigation of these interaction phenomena.

4. Test of Literature Interaction Indicators

The findings of the previous subsection were obtained because the system was simple enough to allow an analysis of eigenvalues and identification of the dominant mode via a parametric sensitivity study. However, in a bigger, more realistic and complex system, the pole map may not be as straightforward to interpret. Therefore, an interaction indicator accounting for the participation factors to identify the eigenvalue encasing the instability mechanisms would be needed.

In this section, the conclusions that could be drawn from the application of the literature interaction indicators are confronted to the previously established interaction study.

Three indicators are selected for this section: the Interaction Index (IntI), the Risky Interaction Index (RIntI) and the Converter Interaction Parameter (CIP) from [6], [7].

4.1. Interaction Index

The IntI [6] is calculated as follows for two subsystems (k_1, k_2), for a given eigenvalue λ_i :

$$IntI_i = \sqrt{\max(PF_{i,k1})^2 + \max(PF_{i,k2})^2} \quad (2)$$

where $PF_{i,k1}$, $PF_{i,k2}$ are the vectors of the participation factors of the state variables belonging to the subsystems k_1, k_2 respectively.

For each combination, IntI is calculated for all eigenvalues and the eigenvalue with the highest indicator is selected as the eigenvalue to study closer thereafter.

For the proposed test setup, three combinations of subsystems are possible: Grid-VSC1, Grid-VSC2, VSC1-VSC2.

Table 4. Flagged eigenvalues by the IntI for each subsystems combination

Grid-VSC1	Grid-VSC2	VSC1-VSC2
-10.37	-300	-300

As shown in Table 4, the IntI does not flag ($\lambda = -27.11 \pm 111.71i$) for any combination of the subsystems. In fact, considering how the indicator is defined, it is sufficient for an eigenvalue to be highly dependent on one of the subsystems to be flagged as an interaction eigenvalue of the combination of both. The eigenvalues flagged here are a clear example as the -10 eigenvalue is representative of the active power bandwidth and the -300 eigenvalues are representative of the outer loops filter cutoff frequency.

To conclude, the IntI fails to identify the eigenvalue reflecting the system dominant behavior and mistakes harmless eigenvalues due to common tuning parameters as interaction phenomena.

4.2. Risky Interaction Index

The RIntI [6] is proposed to overcome the downsides of the IntI by weighing the IntI of each eigenvalue by its damping ratio to discard the eigenvalues that are well damped and represent no risk to the system dynamic.

The RIntI is calculated as follows for two subsystems (k_1, k_2), for a given eigenvalue λ_i :

$$RIntI_i = (1 - \xi_i) \cdot \sqrt{\max(PF_{i,k1})^2 + \max(PF_{i,k2})^2} \quad (3)$$

where ξ_i is the damping of the eigenvalue λ_i and $PF_{i,k1}$, $PF_{i,k2}$ are the vectors of the participation factors of the state variables belonging to the subsystems k_1, k_2 respectively.

Table 5. Flagged eigenvalues by the RIntI for each subsystems combination

Grid-VSC1	Grid-VSC2	VSC1-VSC2
-143 ± 639i	-143 ± 639i	-27 ± 117i

As shown in Table 5, the RIntI successfully identifies the eigenvalues of interest for the VSC1-VSC2 subsystems combinations. Incidentally, the other identified eigenvalue corresponds to the other pair of eigenvalues that shows a high sensitivity to grid strength as show in figure 6.

Looking closer at the participation factors of this eigenvalue, shown in figure 9, the previously identified downside of the IntI appears to remain a property of the RIntI: it is enough for one of the subsystems (here, the grid) to significantly contribute to a given eigenvalue for it to be flagged as an interaction eigenvalue. Such a property causes misleading readings of what could be considered as interactions phenomena.

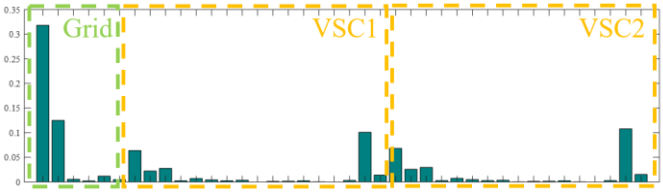

Fig. 9. Participation factors of state variables in $\lambda_2 = -143 \pm 639i$.

4.3. Converter Interaction Parameter

The CIP [7] is calculated for every eigenvalue for every subsystem. For a given eigenvalue λ_i and a subsystem k :

$$\eta_{k,i} = \frac{\|PF_{i,k}\|_{L1}}{\|PF_i\|_{L1}} \quad (4)$$

where $\|PF_{i,k}\|_{L1}$, $\|PF_i\|_{L1}$ are respectively, the L^1 norm of the vector of the participation factors of the state variables belonging to the subsystems k, and the vector of the participation factors of the full system state variables.

An eigenvalue is considered worth investigating as an interaction mode of two given subsystems k_1, k_2 if:

$$\begin{cases} \eta_{k1,i} > \alpha \\ \eta_{k2,i} > \alpha \end{cases}$$

where α is a chosen threshold. Therefore, the issue of flagging eigenvalues due to the dominance of the participation of one subsystem, previously encountered with IntI and RIntI, can be avoided.

The value of this threshold significantly impacts the number of flagged eigenvalues and is adapted depending on the number of state variables and the complexity of the system under study. For example, a 5% threshold is chosen in [7]. However, for the system studied in the present work, any threshold below 40% would lead to more than 25% of the eigenvalues getting flagged which goes against the purpose of using indicators to reduce the number of eigenvalues to closely analyze.

For a threshold set at 40%, no eigenvalues are flagged for the combinations of subsystems containing the grid. The combination of both converters flags nine eigenvalues, five of which have a null imaginary part. The remaining four are two pairs of conjugate poles $(-11 \pm 1i, -954 \pm 1415i)$. By looking into the participation factors of theses eigenvalues, it is revealed that they do not reflect interaction phenomena but rather the identical tuning of the converters with regards to the outer loops and the output delay.

5. Conclusions

The present work has shown the limit of the studies conducted on the Thévenin equivalent and proposed an alternative that allows a better understanding of interaction phenomena. Using the proposed setup, it was possible to pinpoint the small-signal stability limit of the controls without reaching the static limit of the setup. The small-signal stability analysis showed the interaction phenomena by first identifying the dominant mode via parametric sensitive study, then by analyzing its participation factors. This same analysis could not have been replicated when using the interactions indicators from the literature as they flagged the wrong eigenvalues. However, there could be interest in combining the CIP with the RIntI by

weighing the CIP indicator with the eigenvalues damping to filter out the damped modes resulting from the potentially identical control tuning.

6. REFERENCES

[1] ENTSO-E, "Stability Management in Power Electronics Dominated Systems: A Prerequisite to the Success of the Energy Transition." Jun. 2022.

[2] J. Z. Zhou, H. Ding, S. Fan, Y. Zhang, and A. M. Gole, "Impact of Short-Circuit Ratio and Phase-Locked-Loop Parameters on the Small-Signal Behavior of a VSC-HVDC Converter," *IEEE Trans. Power Deliv.*, vol. 29, no. 5, pp. 2287–2296, Oct. 2014, doi: 10.1109/TPWRD.2014.2330518.

[3] R. Rosso, M. Andresen, S. Engelken, and M. Liserre, "Analysis of the Interaction Among Power Converters Through Their Synchronization Mechanism," *IEEE Trans. Power Electron.*, vol. 34, no. 12, pp. 12321–12332, Dec. 2019, doi: 10.1109/TPEL.2019.2905355.

[4] J. F. Morris, K. H. Ahmed, and A. Egea-Àlvarez, "Analysis of Controller Bandwidth Interactions for Vector-Controlled VSC Connected to Very Weak AC Grids," *IEEE J. Emerg. Sel. Top. Power Electron.*, vol. 9, no. 6, pp. 7343–7354, Dec. 2021, doi: 10.1109/JESTPE.2020.3031203.

[5] W. Wang *et al.*, "Instability of PLL-Synchronized Converter-Based Generators in Low Short-Circuit Systems and the Limitations of Positive Sequence Modeling," in *2018 North American Power Symposium (NAPS)*, Sep. 2018, pp. 1–6. doi: 10.1109/NAPS.2018.8600590.

[6] C. Collados-Rodriguez, M. Cheah-Mane, E. Prieto-Araujo, and O. Gomis-Bellmunt, "Stability and operation limits of power systems with high penetration of power electronics," *Int. J. Electr. Power Energy Syst.*, vol. 138, p. 107728, Jun. 2022, doi: 10.1016/j.ijepes.2021.107728.

[7] J. Beerten, S. D'Arco, and J. A. Suul, "Frequency-dependent cable modelling for small-signal stability analysis of VSC-HVDC systems," *IET Gener. Transm. Distrib.*, vol. 10, no. 6, pp. 1370–1381, Apr. 2016, doi: 10.1049/iet-gtd.2015.0868.